BJ Biomolecules

Biochem. J. (2014) **462**, 441–452 (Printed in Great Britain) doi:10.1042/BJ20140382

online data

Structural and functional characterization of ochratoxinase, a novel mycotoxin-degrading enzyme

Doreen DOBRITZSCH*†[1], Huaming WANG‡§, Gunter SCHNEIDER* and Shukun YU¶‖[1]

*Department of Medical Biochemistry and Biophysics, Karolinska Institutet, SE-17177 Stockholm, Sweden
†Department of Chemistry, BMC, Uppsala University, SE-75123 Uppsala, Sweden
‡Genencor, Danisco A/S (DuPont), Palo Alto, CA 94304, U.S.A.
§Tianjin Institute of Industrial Biotechnology, Chinese Academy of Science, 300308 Tianjin, China
¶Genencor, Danisco A/S (DuPont), DK-8220 Brabrand, Denmark
‖Department of Biotechnology, Lund University, SE-22100 Lund, Sweden

Ochratoxin, with ochratoxin A as the dominant form, is one of the five major mycotoxins most harmful to humans and animals. It is produced by *Aspergillus* and *Penicillium* species and occurs in a wide range of agricultural products. Detoxification of contaminated food is a challenging health issue. In the present paper we report the identification, characterization and crystal structure (at 2.2 Å) of a novel microbial ochratoxinase from *Aspergillus niger*. A putative amidase gene encoding a 480 amino acid polypeptide was cloned and homologously expressed in *A. niger*. The recombinant protein is N-terminally truncated, thermostable, has optimal activity at pH ∼6 and 66 °C, and is more efficient in ochratoxin A hydrolysis than carboxypeptidase A and Y, the two previously known enzymes capable of degrading this mycotoxin. The subunit of the homo-octameric enzyme folds into a two-domain structure characteristic of a metal dependent amidohydrolase, with a twisted TIM (triosephosphateisomerase)-barrel and a smaller β-sandwich domain. The active site contains an aspartate residue for acid–base catalysis, and a carboxylated lysine and four histidine residues for binding of a binuclear metal centre.

Key words: metal-dependent amidohydrolase, mycotoxin, ochratoxin degradation, protein crystal structure.

INTRODUCTION

Mycotoxins are secondary metabolites produced by fungi. Several hundred mycotoxins are currently documented, with aflatoxin, ochratoxin, fumonisin, deoxynivalenol and zearalenone being the most toxic and consequently the best studied. Aflatoxin and ochratoxin are known as Nature's most-toxic compounds as they act at ppb (parts-per-billion) levels. They frequently occur in a wide range of agricultural commodities [1,2] and thus represent a major threat to human and animal health.

Ochratoxins are derivatives of isocoumarin produced by several species of the *Aspergillus* or *Penicillium* genera [3]. They are named after *Aspergillus ochraceus* and occur in three isoforms designated ochratoxin A, B and C. OTA (ochratoxin A; Scheme 1) is the most abundant and potent of these, showing nephrotoxic, teratogenic, hepatotoxic and carcinogenic effects [4]. OTA can occur in, for example, cereals, pulses, grapes, coffee and meat products of non-ruminant animals exposed to contaminated feedstuffs [3]. To reduce the risk of human exposure to one of Nature's most harmful toxins, many countries have set limits on OTA levels in food, typically between 2 and 50 ppb [5]. Biodegradation of OTA by micro-organisms or enzyme preparations is an attractive means of food detoxification, because it is highly target-specific, environmentally friendly, potentially efficient and likely to preserve food product quality [6]. Several micro-organisms have been identified as capable of detoxifying OTA, either by biodegradation or adsorption into their cell walls. The latter is suggested to be the primary mechanism by which lactic acid bacteria and yeasts detoxify OTA [7,8]. Biodegradation of OTA may be achieved by different pathways in different organisms [9], with hydrolysis, hydroxylation, lactone ring opening and conjugation to other entities as the major initial reaction steps. In contrast with lactone ring opening, hydrolysis of the amide bond between the phenylalanine and ochratoxin α moieties of OTA results in products that are little or essentially non-toxic (Scheme 1). It has been estimated that ochratoxin α is 1000-times less toxic in brain cell cultures and that its elimination half-life *in vivo* is 10-times faster than for OTA [3].

Hydrolysis of OTA has been reported to occur in animals and humans, rumen protozoa, and specific strains of bacteria [10], yeast [11] and filamentous fungi (e.g. *Aspergillus niger*). Only a few enzymes capable of degrading OTA are, however, known, and less have been isolated and further characterized. Bovine pancreatic CPA (carboxypeptidase A) was the first enzyme reported to hydrolyse the OTA amide bond, although at low efficiency [12,13]. The enzyme hydrolyses ochratoxin B, the dechlorinated derivative, 10-times faster than the parent compound [13,14], which may explain why animals that have CPA in the digestive tract are still liable to OTA toxicity [4]. The OTA-hydrolysing activity of yeast carboxypeptidase Y is even lower than that of CPA [3]. Hydroxylation of OTA to 4-(*R*)-hydroxy or 4-(*S*)-hydroxy derivatives reported to occur in rodents and pig respectively, involves cytochrome P450 enzymes or peroxidases [14a]. Further reports of OTA-degrading activity concern crude enzyme preparations, with the active component of these preparations neither being unambiguously identified

Abbreviations: ASS, active site segment; CPA, carboxypeptidase A; 4MF, *N*-(4-methoxyphenylazoformyl)-phenylalanine; NCS, non-crystallographic symmetry; OTA, ochratoxin A; OTase, ochratoxinase; ppb, parts-per-billion.

[1] Correspondence may be addressed to either of these authors (email Doreen.Dobritzsch@kemi.uu.se or Shukun.Yu@biotek.lu.se).

The crystallographic data and structures described in the present paper have been deposited in the PDB under codes 4C5Z (OTapo-h), 4C5Y (OTholo-h), 4C60 (OTapo-l1) and 4C65 (OTapo-l2).

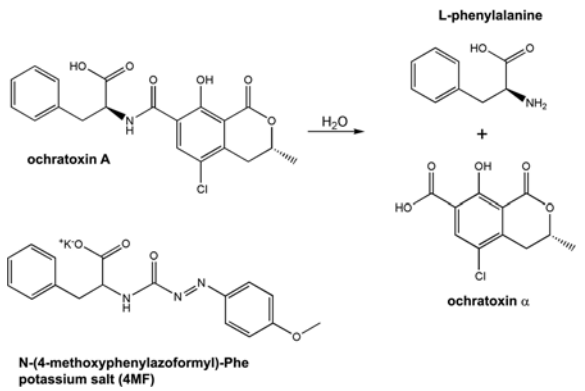

Scheme 1 Structural formulas of OTA, the products of OTA amide bond hydrolysis and the OTA analogue 4MF

nor purified. Stander et al. [15] first reported the commercial product "Amano™ lipase" from *A. niger* (Amano Enzyme) to have ochratoxin-degrading side activity. Since the further purified product was also active towards *p*-nitrophenyl palmitate it was concluded that its lipase component was responsible for the OTA degradation. Abrunhosa et al. [16,17] reported ochratoxin-degrading activity of *A. niger* when cultured with OTA as a carbon and nitrogen source, and suggested the responsible enzyme to be a metalloenzyme.

In an effort to find microbial enzymes that can degrade ochratoxins more efficiently than carboxypeptidases A and Y the Amano™ lipase preparation was analysed further to isolate the OTA active fraction. Two of its minor components were sequenced and found to be related to hypothetical amidases encoded by *A. niger* ORFs. In the present paper we report the cloning, purification and characterization of one of these amidases, which is demonstrated to have OTA-hydrolysing activity and thus represents the first identified microbial OTase (ochratoxinase). Furthermore, we determined the crystal structure of *A. niger* OTase at 2.2 Å resolution.

EXPERIMENTAL

Materials

OTA (catalogue number 32937), *Citrus sinensis* peptide amidase (catalogue number 17232) and penicillin amidase (catalogue number 76429) were purchased from Fluka. Bovine pancreatic CPA (catalogue number C9268), carboxypeptidase Y from baker's yeast (catalogue number C3888), the CPA assay kit (catalogue number CS1130), hippuryl-L-phenylalanine (catalogue number H6875), formamide (99.8 %; catalogue number F9037), *N*,*N*-dimethylformamide (99.9%; catalogue number D4551), *Pseudomonas aeruginosa* amidase (catalogue number A6691) and CelLytic™ Y Cell Lysis Reagent (catalogue number C4482) were obtained from Sigma–Aldrich. Amano lipase A from *A. niger* (catalogue number 53781) was from Amano Enzyme via Sigma–Aldrich. A formic acid assay kit (K-Form) was obtained from Megazyme. All other enzymes and reagents were purchased from Roche, Merck and Danisco (DuPont). Chromatography equipment and column materials were from GE Healthcare, microtitre plates from Nunc A/S and Corning, NuPAGE 4–12 % Bis-Tris gels from Invitrogen, and the microplate reader from BioTek.

Cloning

An expression plasmid was constructed for an *A. niger* UVK143 ORF encoding a protein of 480 amino acids. The gene was amplified by Pfu Ultra II PCR (30 cycles of 95 °C for 30 s, 50 °C for 30 s and 72 °C for 1 min) with a genomic DNA template obtained from the *A. niger* UVK143 strain [18], using 5′-GGAGATCTATCATGGTCCGCCGAATTG-3′ and 5′-AATCTAGACTAGTGATGGTGATGGTGATGCAGAAAAGG-ATTACGTG-3′ as the forward and reverse primers respectively. These primers were designed based on An14g0280 (6231–7673 bp) of *A. niger* CBS 513.88 (GenBank® accession number AM270317) [19]. After final extension at 72 °C for 5 min the reaction was chilled to 4 °C. The PCR fragment turned out to have exactly the same length (1443 bp) and sequence as An14g02080 of *A. niger* CBS 513.88 which codes for a protein of 480 amino acids annotated as unnamed protein product of *A. niger* (GenBank® accession number CAP07464.1). It was purified using a Qiagen spin column, digested with BglII and XbaI, and cloned into the pGAPT plasmid vector [20] pre-digested with the same restriction enzymes. The resulting pGAPT-OTase plasmid (Supplementary Figure S1 at http://www.biochemj.org/bj/462/bj4620441add.htm) was subsequently transformed into the *A. niger* AP4 strain [21,22]. It contains the recombinant *A. niger* UVK143 OTase gene inserted between the *A. niger* glucoamylase promoter and an *A. tubingensis* glucoamylase terminator, as confirmed by DNA sequencing.

The *A. nidulans fmd* gene encoding a formamidase protein of 411 amino acids (GenBank® accession number AAG60585) was also cloned. To construct the recombinant expression plasmid, the primers 5′-CCGGATCCATCATGGGTACCAAGGCTATTC-3′ and 5′-GGCTCGAGACCGGTCACTTTGAAGCAAAAG-3′ were used in a Pfu Ultra II PCR with an *A. nidulans* genomic DNA template [23]. The remaining procedures for PCR, vector construction and transformation of the *fmd* were the same as for the *A. niger* CBS 513.88 ORF An14g02080 described above.

Protein expression and purification

A. niger transformants harbouring the OTase gene were grown in shake flasks for 6 days at 28 °C, after which the recombinant protein is accumulated inside the cells as well as in the extracellular fraction, i.e. the fermentation broth. The extracellular fraction was collected as supernatant after centrifugation of the broth at 10 000 ***g*** for 10 min. To release the intracellular fraction the mycelium pellets were twice washed with water, resuspended in CelLytic™ Y Cell Lysis Reagent and lysed according to the manufacturer's instructions at 25 °C for 2 h. After centrifugation at 10 000 ***g*** for 10 min, the obtained supernatant was used for further purification of the enzyme.

The supernatant containing the extracellular protein was fractionated by ammonium sulfate precipitation. The pellet obtained between 40 % and 60 % ammonium sulfate saturation was dissolved in 50 mM Tricine/HCl (pH 7.0) containing 1 M ammonium sulfate (buffer A). The solution was filtered (0.22 μm) and applied on to a Phenyl Sepharose FF column (2.6 cm × 10 cm) equilibrated with buffer A. The column was washed with five column volumes of buffer A before elution of bound proteins with a linear gradient of 50 mM Tricine/HCl (pH 7.0) (buffer B). Fractions with high OTase activity, monitored by reverse-phase HPLC using OTA as a substrate, were pooled, desalted on a PD10 column equilibrated with 20 mM Tris/HCl (pH 7.5) (buffer C), and applied to a Source Q30 column equilibrated with buffer C. Elution was performed with a linear gradient of 0–1 M NaCl in

buffer C. Fractions with OTase activity were concentrated using Amicon Centriprep™ concentrators (10 kDa cut-off) and stored at −20 °C and 5 °C for further use. The intracellular fraction of the recombinant protein as well as the amidases from the Amano lipase product were purified following the same procedure and analysed by SDS/PAGE (NuPAGE 4–12% Bis-Tris gels) and LC–MS.

Protein concentrations were determined using the Bio-Rad Laboratories protein assay reagent (Coomassie Brilliant Blue) and following the manufacturer's protocol by measuring the absorbance at 595 nm with BSA as standard. The molecular mass and purity of the obtained OTase fractions were estimated by SDS/PAGE using NuPAGE 4–12 % Bis-Tris gels. The precise molecular mass was determined using a Bruker Autoflex MALDI–TOF mass spectrometer running in positive linear mode with sinapinic acid as the matrix according to the manufacturer's instruction. The gene product was unambiguously identified by HPLC–MS/MS (Agilent 1100 Cap-LC system) of peptides obtained upon trypsin digestions of the corresponding SDS gel band. The resulting spectra were automatically searched against protein databases using the Mascot search engine.

Enzyme activity assays

Formamidase assay

Formamidase (EC 3.5.1.49) activity was assayed by following the enzymatic release of formic acid from formamide using the Megazyme kit according to the manufacturer's instructions with modifications to reduce the reaction volume from 1-cm light path cuvette to 96-well half-bottom area microplates. This method has a detection limit of 0.4 μg/ml formic acid. The reaction mixture was pipetted from kit components as follows: 10 μl of phosphate buffer (pH 7.6), 10 μl of NAD^+, 2.5 μl of formic acid dehydrogenase, 5 μl of formamidase sample and 100 μl of deionized water. The reaction was started with the addition of 1.5 μl of undiluted formamide or dimethylformamide, and NADH formation was followed at 340 nm and 37 °C for 60 min.

OTase activity assays

Enzymatic hydrolysis of OTA was followed by reverse-phase HPLC, monitoring the disappearance of OTA peaks and appearance of peaks corresponding to the OTA degradation product ochratoxin α with a fluorescence detector, with minor modifications to the procedure described earlier [24]. The method established in our laboratory has a linear range of 25–6000 pg of OTA per injection and a detection limit of 1–2 ppb. It was used routinely to follow OTase activity in the purification steps and to screen *A. niger* transformants for OTA-degrading activities. An OTA stock solution (1 mg/ml) was prepared by dissolving 5 mg of OTA in 60 % (v/v) ethanol and stored at −20 °C. OTase assay reaction mixtures consisted of 245 μl of 1 μg/ml OTA in 50 mM MES (pH 7.0) and 5 μl of OTase sample. The reactions were performed at 40 °C for 30 min and up to 2 h, and stopped by heating at 95 °C for 5 min or by the addition of equal volume of acetonitrile. Filtration of the resulting samples (0.22 μm syringe filter) was followed by application of 5 μl of filtrate to a nucleosil 100-5 C_{18} column (250 mm×4.6 mm; Chrompack) on a Dionex HPLC. Elution was performed with water/acetonitrile/acetic acid (100:100:1, by vol.) at 0.6 ml/min and 30 °C. OTA and its degradation product ochratoxin α were monitored by UV (235 nm) and fluorescence ($\lambda_{ex} = 278$ nm and $\lambda_{em} = 440$ nm) spectroscopy.

For determination of the pH dependence of OTase activity, 67 mM phosphate buffer with a pH range 3.0–9.0 was used. Reactions were performed at 37 °C for 30 min and stopped as described above. Standard OTA degradation assays were subsequently performed under optimum conditions.

OTase activity was also determined based on an OTA-specific monoclonal antibody technique using the competitive enzyme immunoassay kit RIDASCREEN®FAST Ochratoxin A from R-Biopharm (detection range of 5–50 ppb). The reaction mixture contained 10 μl of OTA (10 μg/ml), 10 μl of the OTA-degrading enzyme (containing 0.07 μg of OTase or 6.7 μg of bovine pancreatic CPA), 50 μl of 0.2 M Mops/HCl (pH 7.5) and 30 μl of water. Reactions were carried out in triplicate at 40 °C for 0, 20, 40 and 60 min, and stopped by heating at 100 °C for 5 min. The reaction mixtures were diluted 25 times with water/ethanol (97.5:2.5), and 50 μl of the diluted samples were assayed for residual OTA according to the manufacturer's instruction.

Considering the biohazard of working with OTA, and because only discontinuous assays could be performed for OTA hydrolysis, purified OTase was also assayed with the OTA analogue 4MF [*N*-(4-methoxyphenylazoformyl)-phenylalanine] as a substrate. The decrease in absorption at 350 nm caused by 4MF ($\varepsilon_{350} = 19\,000$ $M^{-1}\cdot cm^{-1}$) hydrolysis was followed spectrophotometrically. Reactions were performed at 30 °C and pH 6.0 in a 96-well microtitre plate using a concentration range of 8.4–670 μM 4MF. Use of higher 4MF concentrations was hampered by the strong absorbance of the substrate, exceeding the limits of reliable detection by the spectrophotometer and the range of linear absorbance–concentration dependence. The reaction mixture (final volume = 100 μl) consisted of 50 μl of GAT [a composite buffer system consisting of 50 mM glycine, 50 mM acetic acid and 50 mM Tris (pH 6.0)], 5 μl of 0.1 M EDTA, 40 μl of 4MF and 5 μl of OTase. All measurements were performed at least in triplicate. The apparent kinetic parameters K_m^{app} and V_{max}^{app} for 4MF hydrolysis by OTase were estimated from non-linear fitting of the v/[S] plot to Michaelis–Menten kinetics.

For determination of the pH dependence of 4MF hydrolysis, GAT buffer with a pH range 2.5–9.0 was used. Reactions ($n = 4$) were performed at 30 °C and followed spectrophotometrically at 350 nm. The reaction mixture consisted of 40 μl of buffer, 2 μl of appropriately diluted OTase, 59 μl of water and 0.8 μl of 20 mM 4MF. The optimal temperature for 4MF hydrolysis was determined by incubation of tubes containing 95 μl of GAT buffer (pH 6.0), 0.8 μl of 20 mM 4MF and 2 μl of appropriately diluted OTase at six temperatures in the range 20–80 °C for exactly 10 min. The reactions ($n = 4$) were stopped by the addition of 100 μl of 0.25 M glycine/HCl (pH 2.5) and cooled to 20 °C, before 175 μl was taken for absorbance measurement at 350 nm. Blank values were obtained by omitting OTase from the reaction mixture. For thermostability measurements, tubes containing 5 μl of OTase, 5 μl of 0.15 M phosphate buffer (pH 6.9) and 10 μl of 15 % (v/v) glycerol were incubated at 80 °C for 0, 1, 2, 3, 4, 5, 6, 7, 8 and 10 min and immediately placed in ice-cold water. Residual OTase activity was assayed by transferring 6 μl of this mixture to microtitre plate wells containing 34 μl of GAT buffer (pH 6.0), 0.8 μl of 20 mM 4MF and water (final volume 100 μl) and following the absorbance decrease at 350 nm and 30 °C for 25 min. Average maximum reaction rates ($\Delta A = 10^{-3}$ min^{-1}) were obtained from two independent experiments.

Crystallization

For crystallization experiments the purified protein was concentrated by centrifugation in Vivaspin concentrators (10 kDa cut-off) at 6000 ***g*** and 4 °C until it started to precipitate (final

Table 1 Data collection and refinement statistics

Values in parentheses are for the highest resolution shell.

Parameter	OTapo-h	OTholo-h	OTapo-l1	OTapo-l2
Data collection				
Wavelength (Å)	0.976	0.976	0.976	0.933
Space group	$P42_12$	$P42_12$	$I2$	$I2$
X-ray source	ID29	ID29	ID29	ID14-1
Unit cell dimensions				
a, b, c (Å)	183.9, 183.9, 79.9	183.2, 183.3, 79.0	212.7, 79.9, 218.3	210.9, 78.9, 217.0
β (°)	–	–	105.3	105.1
Resolution (Å)	92.0–2.5 (2.64–2.50)	72.5–3.0 (3.16–3.00)	74.7–2.5 (2.64–2.50)	37.8–2.2 (2.24–2.20)
Multiplicity	9.6 (9.7)	5.5 (5.7)	2.5 (1.9)	2.7 (2.7)
R_{merge} (%)	18.2 (61.1)	19.7 (74.6)	10.1 (35.8)	10.4 (47.8)
Mean $[I/\sigma(I)]$	9.4 (3.3)	6.3 (2.2)	5.7 (2.1)	6.1 (2.0)
Completeness (%)	96.5 (97.6)	96.2 (97.2)	91.0 (70.5)	87.7 (73.4)
Wilson B-factor (Å^2)	36.1	62.9	42.3	20.5
Number of reflections				
Overall	441395 (65195)	145992 (21722)	273425 (24287)	413362 (16895)
Unique	46056 (6711)	26324 (3842)	111178 (12486)	153345 (6284)
Refinement				
Number of reflections working/test set	43557/2380	24926/1341	105606/5524	145645/7696
Resolution (Å)	73.3–2.5	67.5–3.0	74.7–2.5	37.8–2.2
R-factor/R_{free} (%)	17.5/20.9	18.8/22.6	20.6/23.1	21.3/24.5
Number/average B-factor (Å^2)				
Protein atoms	6527/36.6	6516/59.4	26062/34.7	26060/28.0
Water molecules	370/28.4	31/29.9	638/21.1	1240/19.7
Zinc ions	–	4/102.3	–	–
RMSD				
Bond lengths (Å)	0.011	0.011	0.009	0.011
Bond angles (°)	1.44	1.44	1.34	1.43
Ramachandran plot				
Residues in favoured regions (%)	96.5	97.0	96.8	96.5
Residues in allowed regions (%)	3.2	2.8	3.2	3.5
Residues in outlier regions (%)	0.2	0.2	0	0

concentrations of 2.9–4.2 mg/ml), with a concomitant exchange of the sample buffer to 20 mM Tris (pH 7.5) and 50 mM NaCl. Initial crystallization screens were performed using 96-well sparse matrix screens and nano-drop robotics in sitting-drop setups at 20 °C. Approximately 15 of the 184 tested conditions produced crystals. All crystals used for data collection were obtained by hanging drop vapour diffusion against 1 ml reservoirs at 20 °C. The 2 μl hanging drop consisted of equal volumes of reservoir and protein solution [2.9 mg/ml OTase in 20 mM Tris (pH 7.5) and 50 mM NaCl]. Crystals resulting in datasets OTapo-h (h stands for high pH) and OTholo-h were grown using a reservoir solution of 10–12 % (w/v) PEG 3000, 0.2 M tri-potassium citrate and 0.1 M of either Tris (pH 8.5) or Bicine (pH 9.0). Datasets OTapo-l1 and OTapo-l2 (l stands for low pH) were collected from crystals obtained under the same conditions, but with the buffer component exchanged to citrate (pH 5.0). For OTapo-l2, the protein solution was supplemented with 3 mM 4MF (Scheme 1) and 100 μM $ZnCl_2$. Crystals appeared within 1–2 days of equilibration.

Data collection, structure determination and refinement

Crystals were transferred to a cryo-protectant solution, consisting of 70–75 % (v/v) of the respective reservoir solution and 25–30 % (v/v) glycerol, ethylene glycol or PEG 400, for 1–5 s and flash-frozen by plunging into liquid nitrogen. For cryo-protection of the OTholo-h crystal the cryo solution was supplemented with 10 mM 4MF and 100 μM $ZnCl_2$ and the soaking time was increased to 7 min.

Crystallographic data were collected at 100 K at the ID14-EH1 or ID29 beamline of the European Synchrotron Radiation Facility (Grenoble, France). Details of data collection and statistics are given in Table 1. The OTapo-h and OTholo-h crystals belong to space group $P42_12$, with unit cell parameters of $a = b = 183.9$ Å and $c = 79.9$ Å. The diffraction quality of the latter deteriorated rather rapidly during exposure, possibly due to weakening of the crystal lattice by soaking-induced conformational changes (see below). The asymmetric unit contains two identical polypeptide chains. The OTapo-l1 and OTapo-l2 crystals grown at lower pH belong to space group $I2$, with eight subunits per asymmetric unit. Integration of all diffraction data was carried out with iMOSFLM [25]. Intensities were merged and scaled using SCALA or AIMLESS [26] and structure factors amplitudes were calculated with CTRUNCATE of the CCP4 suite of programs [27].

Phases were obtained by molecular replacement using PHASER [28]. An ensemble of five superimposed subunit structures of known and putative peptidases and amidases that show 30–35 % sequence identity to OTase (PDB codes 3BE7 [29], 3FEQ, 3MTW, 3MKV [30] and 2QS8 [31]) was used as the search model. Phasing was performed with the OTapo-h data in the range of 73.3 to 2.8 Å, resulting in a clear solution placing two subunits in the asymmetric unit.

After initial rigid body and restraint refinement and extension of the phases to 2.5 Å resolution, iterations of model building in COOT [32] were alternated with TLS (Translation–Libration–Screw-rotation) and restrained refinement in REFMAC5 [33] until crystallographic R-factor and R_{free} converged. All reflections in the given resolution range (Table 1) were used with the exception of 5 % for monitoring R_{free}. Initially, tight NCS (non-crystallographic symmetry) restraints were applied to all main chain atoms except those belonging to two flexible loops near the active site. During

the final cycles of the refinement automatically determined local NCS restraints were applied. Water molecules were added using the search routine implemented in COOT.

Initial models for datasets OTholo-h, OTapo-l1 and OTapo-l2 were obtained by molecular replacement using the subunit of the refined OTapo-h structure as a search template. Model building and crystallographic refinement were performed as for OTapo-h. The refined models are either of higher resolution than OTapo-h (OTapo-l2), show structural deviations (all) or metal-centre binding (OTholo-h).

All refined models have good stereochemistry as determined with RAMPAGE [34] and MOLPROBITY [35], with >95 % of the residues in the favoured and 0–0.2 % in the disallowed regions of the Ramachandran plot. Details regarding the model content and quality are given in Table 1. Structure comparisons and similarity searches were performed using LSQKAB [36] and the Protein Structure Comparison service SSM at the European Bioinformatics Institute (http://www.ebi.ac.uk/msd-srv/ssm) [37]. Molecular surfaces were analysed using PISA at the European Bioinformatics Institute (EBI) [38]. Cavities were calculated with the CASTp server using default parameters [39]. Figures 2–5 and Supplementary Figures S2 and S3 were prepared using PyMOL (http://www.pymol.org). The crystallographic data and structures have been deposited in the PDB under codes 4C5Z (OTapo-h), 4C5Y (OTholo-h), 4C60 (OTapo-l1) and 4C65 (OTapo-l2).

RESULTS AND DISCUSSION

Identification and characterization of *A. niger* OTase

First, the Amano lipase A preparation was separated by ammonium sulfate fractionation and chromatographic steps to isolate the OTA active fraction. Tryptic digest and LC–MS analysis of SDS/PAGE protein bands revealed that this fraction contains a number of different enzymes, including acetylesterase, aldose 1-epimerase, glutamyltranspeptidase, a putative formamidase and the hypothetical protein encoded by An14g02080 with sequence similarity to bacterial amidases. Since OTA-hydrolysing enzymes are likely to be amidohydrolases, the two putative amidases were the strongest candidates for catalysing the OTA breakdown by the lipase product.

Next, commercially available amidases active on C–N bonds were tested for their capability of hydrolysing OTA, including *Citrus sinensis* peptide amidase, *Pseudomonas aeruginosa* amidase and penicillin amidase. None of them showed OTase activity, indicating that the OTA-hydrolysing amidase was specific and might originate from *A. niger*. Therefore we cloned and expressed genes for the two amidases found in the Amano lipase product, namely the *A. niger* CBS 513.88 An14g02080 gene and the *A. nidulans* formamidase gene *fmdA*. The latter was chosen because it had been studied for its expression under various nutrition conditions [23], but has not yet been tested for OTase activity. Its amino acid sequence is 91 % identical and of similar length (411 compared with 413 amino acids) compared with the putative *A. niger* formamidase (GenBank® accession number EHA24058). Both genes were successfully expressed in *A. niger*. Some transformants harbouring the *A. nidulans fmdA* gene showed formamidase activity in the extracellular fractions that was 20-40-times higher than the control (i.e. *A. niger* transformed with empty vector). However, their activity towards OTA was for both the intra- and extra-cellular fractions not proportional to the formamidase activity (results not shown), allowing the tentative conclusion that the *A. niger* formamidase in the lipase product was not responsible for OTA degradation. In contrast, some transformants containing the *A. niger* UVK143 gene for the putative amidase showed OTase activity higher than the control, decreasing the OTA concentration below the detection level (1–2 ppb), i.e. below the regulatory limit [5], when 10 μl of either extra- or intra-cellular fraction was incubated with 185 ppb OTA in 67 mM phosphate (pH 7.0) for 35 min at 40 °C. Sequencing of the gene (deposited in GenBank® under accession number KJ854920) revealed that it is 1443 bp in length, intron free and completely identical in sequence to the An14g02080 gene of *A. niger* CBS 513.88 (GenBank® accession number AM270317) [19]. The corresponding putative amidase was subsequently purified from the fermentation broth of the most active transformant by ammonium sulfate fractionation, hydrophobic interaction and anion-exchange chromatography. The purest fraction from the last purification step was used for all further studies.

The molecular mass of the purified extracellular amidase estimated by SDS/PAGE (~47 kDa) and determined by MALDI–TOF-MS (47215 Da) deviates from the theoretical mass of 51167 Da calculated for the gene-encoded 480 amino acid polypeptide chain. Peptide mass fingerprinting revealed that this mass difference is caused by an N-terminal truncation of the protein, with the first identified residue being Ser^{43}. This truncation was reproducibly observed for extracellular protein from different batches of fermentations and subsequently also in purified intracellular *A. niger* amidase (Figure 1A). The purpose of the N-terminal sequence of ~40 amino acids is currently unclear as it lacks any recognizable signal peptide motif. However, secretion in the absence of a signal peptide has been observed before, e.g. for *A. niger* aspartic proteases [40]. We annotated the hypothetical *A. niger* CBS 513.88 An14g02080 protein in the database as amidohydrolase 2 or amidase 2 to differentiate it from all other *A. niger* amidases reported at that time to which it showed no sequence homology [41]. Since then genome sequencing efforts have led to the identification of one homologue, a putative amidase from *Aspergillus kawachi* IFO 4308 with 95 % identical amino acid sequence [42] that has not been characterized further. The type of catalysed reaction classifies the purified protein as a member of enzyme class 3 (hydrolases) with a possible Enzyme Commission number of EC 3.5.1.-. On the basis of the observed ochratoxin-hydrolysing activity we tentatively refer to it as ochratoxinase (OTase).

Catalytic properties of OTase

The commercial lipase product of *A. niger*, with lipase as the major component and the band for OTase being invisible on a Coomassie Blue-stained SDS gel, showed similar activity towards OTA hydrolysis as bovine pancreatic CPA on a mg/ml protein basis (results not shown). In order to compare the purified recombinant OTase with this thus far most efficient OTA-degrading enzyme, OTase activity was assayed at pH 7.5, the optimal pH for CPA, using the OTA antibody assay kit. After 60 min incubation with 50 ppb OTA, 0.7 μg/ml (15 μM) OTase had decreased substrate concentrations to 25 ppb, whereas 67 μg/ml (1.4 mM) CPA decreased OTA levels only to 46 ppb. This indicates that the OTase identified in the present study is approximately 600-times more active than CPA in OTA hydrolysis.

Considering the high toxicity of OTA and the inconveniences connected to the discontinuity of OTA hydrolysis assays, the use of safer alternative substrates was explored that would allow continuous monitoring of OTase activity in routine assays. No increase in absorbance at 340 nm connected to NAD^+

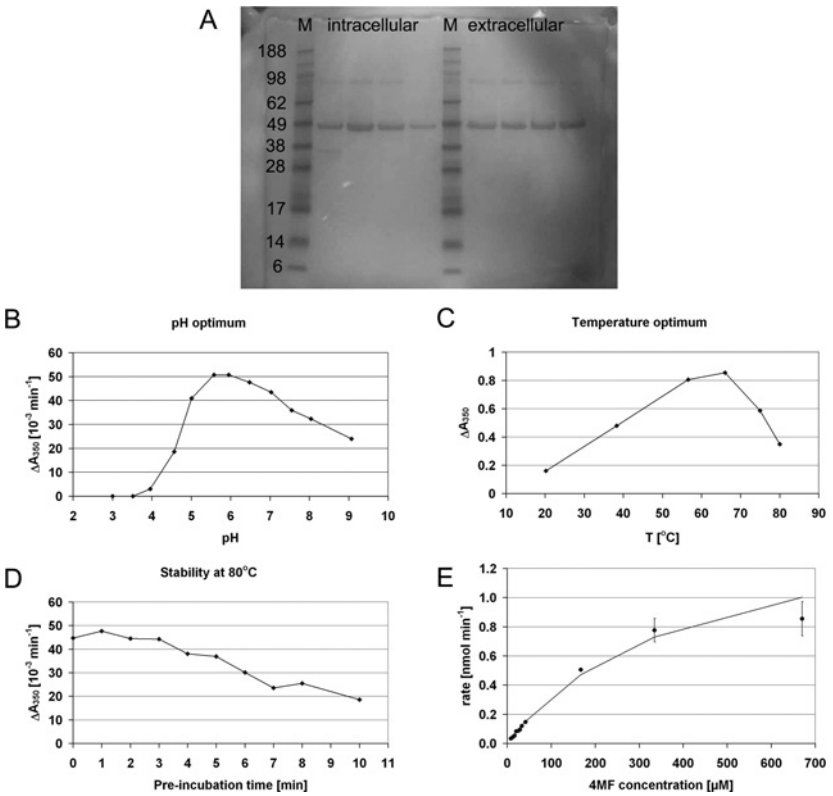

Figure 1 OTase purification and catalytic properties

(**A**) SDS/PAGE of selected intra- and extra-cellular OTase fractions obtained after purification. Lanes labelled with M contain a protein ladder as the marker, with the molecular masses of the respective proteins given in kDa. (**B**) pH dependence of OTase catalytic activity assayed with 4MF as a substrate. The given absorbance changes were observed after 10 min of incubation of enzyme with substrate. (**C**) Temperature dependence of OTase catalytic activity assayed with 4MF as a substrate. (**D**) Stability of OTase at 80 °C and pH 6.9. (**E**) Plot of initial reaction velocities (means ± S.D. from three measurements) against 4MF concentration. The solid line represents the non-linear fit of the primary data to the equation for Michaelis–Menten kinetics.

reduction in a formamidase assay was observed when formamide or dimethylformamide was incubated with OTase at 30 °C for 10 min. In contrast, incubation with *N*-formyl-L-phenylalanine, L-phenylalanyl-L-tyrosine, L-arginyl-L-phenylalanine, hippuryl-L-phenylalanine and 4MF, which like OTA all contain a phenylalanine moiety and are artificial substrates of CPA, resulted in release of free phenylalanine as monitored by increased absorbance at 254 nm or by HPLC (results not shown). We subsequently used the considerably less toxic 4MF as an alternative substrate to conveniently follow the OTase-catalysed reaction via a decrease in its strong absorbance at 350 nm upon hydrolysis.

OTase hydrolyses 4MF optimally at pH 5.6–6.0, with initial reaction rates decreasing more dramatically when shifting the pH towards the acidic end of the scale (Figure 1B). At pH 9, approximately 50 % of the maximum activity is retained. The longer reaction times of 10–30 min used in discontinuous assays with OTA as a substrate may explain the slightly higher pH optimum of OTA hydrolysis of 7.0, as OTase is more stable at alkaline than acidic pH. Nevertheless, the same trend in activity decrease is observed when moving to more extreme pH values (results not shown). The optimal temperature for 4MF hydrolysis and a reaction time of 10 min was determined to be approximately 66 °C (Figure 1C). *A. niger* OTase is thermostable and shows no activity loss in a 4MF-based assay when incubated at 80 °C and pH 6.9 for 3 min, and 50 % residual activity after 10 min of incubation (Figure 1D), which is of great advantage for potential future applications in food and feed processing. At 5 °C and neutral pH the enzyme is stable for at least 2 years without loss of activity even at low protein concentration (10 μg/ml).

Precise determination of the kinetic parameters of 4MF hydrolysis was hampered by the strong absorbance at high substrate concentrations. An apparent K_m of ~400 μM and V_{max} of ~1.6 nmol/min was estimated from non-linear fitting of initial reaction rates obtained for the substrate range 8.4–670 μM 4MF at pH 6.0 (Figure 1E).

Incubation of the recombinant *A. niger* OTase with 10 and 20 mM EDTA had no effect on its 4MF-hydrolysing activity as measured in 25 mM Tricine/HCl (pH 7.0). In contrast, the presence of the Zn^{2+}-specific chelator 1,10-phenanthroline at concentrations of 0.25, 0.5, 2.5, 5 and 10 mM completely abolished the enzyme activity under otherwise identical assay conditions (results not shown).

Structure determination and quality of the models

The structure of the extracellular N-terminally truncated *A. niger* OTase (amino acids 43–480) was determined in two different space groups with crystals growing under essentially the same condition except for a varying buffer component and pH. The initial structure determination by molecular replacement was achieved with the OTapo-h data at 2.5 Å resolution in space group $P42_12$. The asymmetric unit contains two identical subunits that are assembled to octamers by crystallographic symmetry.

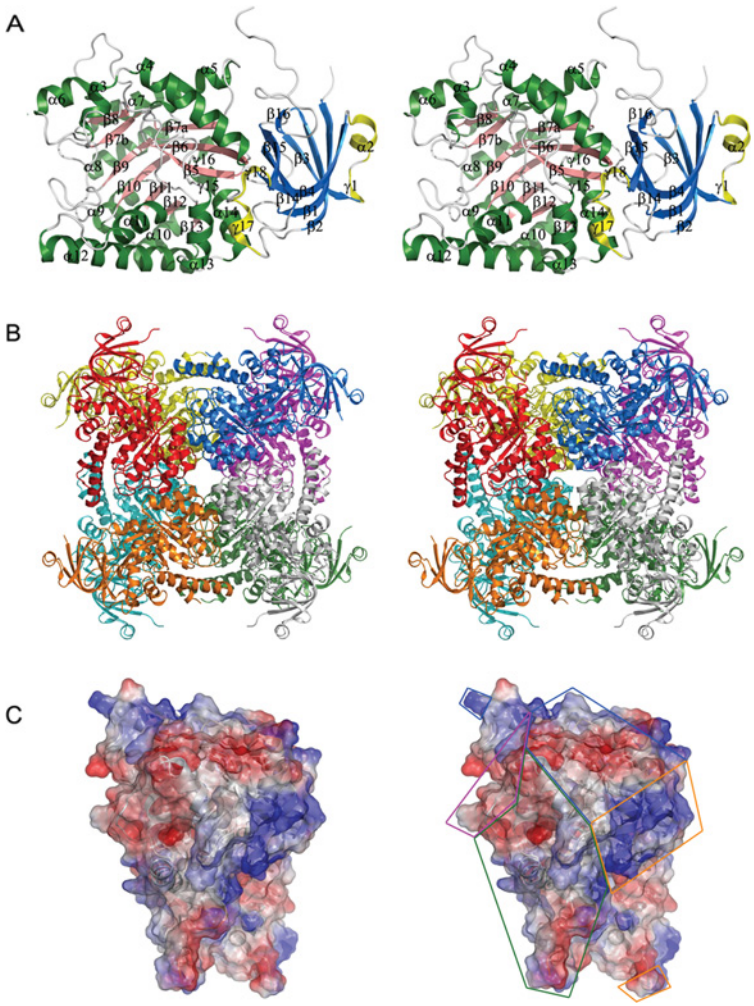

Figure 2 The overall structure of *A. niger* OTase

(**A**) Stereo view of the subunit, with strands and helices of the catalytic domain shown in pink and green, and of the β-sandwich domain in blue and yellow respectively. Strands and helices (α for α-helices and γ for 3_{10}-helices) are numbered consecutively. (**B**) Stereo view of the homo-octamer observed in all crystals of OTase, with subunits coloured differently. (**C**) Stereo view and molecular envelop representation depicting the surface charge distribution for the subunit coloured grey in (**B**). A negative electrostatic potential is indicated by red and positive potential by blue. Right-hand panel: surfaces involved in interface formation with either of the neighbouring dark green, blue, orange and magenta subunits respectively are shown.

Model building was at its final stages when data of equivalent resolution (OTapo-l1) were collected from a crystal belonging to space group *I*2. Its asymmetric unit contains eight polypeptide chains, corresponding to two octamer halves in which subunits are related by four-fold symmetry. The homo-octamer assembled by crystallographic symmetry shows the same overall structure as that observed in space group $P42_12$. The OTholo-h data ($P42_12$) were obtained from a crystal soaked in a cryo-solution supplemented with $ZnCl_2$ and the OTA analogue 4MF for ~7 min before flash-freezing. For OTapo-l2 (*I*2; 2.2 Å resolution) the protein was co-crystallized with both supplements.

The observed electron density was continuous and well-defined for almost the entire polypeptide chains of all four refined models. For some of the chains/models density was lacking or less well defined for residues belonging to two of the loop segments lining the entrance to the active site, termed ASS1 (active site segment 1; residues 251–261) and ASS2 (residues 329–355). The lack of density for two or four residues at the N-terminus is attributed to mobility. The final models were refined to R-values/R_{free} values of 17.5 %/20.9 %, 18.8 %/22.6 %, 20.6 %/23.1 % and 21.3 %/24.5 % for OTapo-h, OTholo-h, OTapo-l1 and OTapo-l2 respectively (Table 1). RMSD values for C_α positions obtained after superimposition of individual subunits are in the range of 0.2 to 0.3 Å for any particular model, and 0.2 to 0.5 Å between models, with the largest deviations observed for the ASSs.

Subunit structure

The fold of the OTase subunit resembles that of other members of the amidohydrolase superfamily [43]. It can be divided into two domains, a core catalytic domain and a smaller β-sandwich domain (Figure 2A). The catalytic domain comprises residues 107–425 forming a distorted TIM (triosephosphateisomerase)-like barrel of eight parallel β-strands (β5–β7 and β9–β13) flanked on the outer face by α-helices. The division of β7 into two strands represents one of the features causing the barrel distortion. Whereas β7a has only one neighbouring barrel strand (β6), β7b is hydrogen-bonded to β8 and β9 of which the former is attached to the barrel core without formally being a part of it. In addition, no hydrogen bonding is observed between residues 375 and 378 directly downstream of β13 and β5 that would close the barrel.

Thus the domain core rather resembles a sandwich of parallel β-sheets, one consisting of three and the other of seven strands. From the 14 helices of the catalytic domain α4, α5, α7–α10 and α12–α13 can be assigned as barrel helices.

The β-sandwich domain comprises residues of both the N- and C-terminus (residues 43–106 and 426–480). The three strands formed by C-terminal residues (β14–β16) are part of the larger of the two sheets. From the strands formed by N-terminal residues β3 belongs to the smaller sheet, and the long and sharply bent β1, β2 and β4 contribute to both sheets, with only β1 and β4 being parallel. Helical turns γ16 and γ17 inserted between β14 and β15 pack against the catalytic domain, whereas helices γ1 and α2 inserted between β3 and β4 are solvent-exposed.

Subunit interactions

In both crystal forms OTase is observed as a homo-octamer with 422 point symmetry and an overall shape resembling a twin propeller (Figure 2B). Both the N- and C-termini of the crystallized extracellular isoform are located on the protein surface, in the groove-like depressions formed between paired sandwich domains. Extension of the N-terminus by ~40 amino acids would thus not necessarily interfere with octamer formation. The octamer can be considered a tetramer of dimers since the largest interface between neighbouring subunits is formed by dimer mates (e.g. the grey and green subunits in Figure 2B). It buries ~1910 Å^2 (~10.2 %) of the solvent-accessible surface area of the subunit and involves residues of both domains, primarily from helices α3–α6 and surrounding loops, strand β8, and the C-terminal tail including γ18. It is dominated by hydrophobic contacts, but also includes a large number of hydrogen bonds and two salt bridges. Details of these interactions are shown in Figure 2(C), and Supplementary Figure S2 and Supplementary Table S1 (http://www.biochemj.org/bj/462/bj4620441add.htm).

In addition, each subunit also interacts with its two neighbours within each tetrameric half as well as with the dimer mate of one of these neighbours (e.g. the blue, orange and magenta neighbours of the grey subunit in Figure 2B). These interfaces bury 940 Å^2 (5.0 %), 1070 Å^2 (5.7 %), and 470 Å^2 (2.5 %) of the accessible surface area per protomer respectively (Supplementary Table S1). Most of the interface-forming residues belong to helices α3 and α6–α8 and adjacent loop regions. The contacts to the neighbouring subunits within a tetrameric half are dominated by electrostatic interactions. The surface patch of the grey subunit that is in contact with the blue subunit is negatively charged due to a number of aspartic and glutamic acid side chains (Figure 2C and Supplementary Figure S2B). The interacting surface of the blue subunit, which corresponds to the grey subunit surface patch contacting the orange subunit, carries a large number of arginine residues and is therefore positively charged. In contrast, no salt bridges and only four hydrogen bonds are observed in the smallest of the interfaces, formed, for example, between the grey and magenta subunits (Supplementary Figure S2C).

Comparison with other protein structures

A search for similar structures resulted in the highest Z-scores for the proteins/enzymes that were selected as search models for molecular replacement based on their sequence homology to OTase. Most of them are not further characterized or putative proteins that are annotated as prolidases, carboxypeptidases or amidohydrolases. For example, the highest Z-score of 17.6 (RMSD of 1.8 Å for 354 aligned Cα atoms) was obtained for Sgx9355e, a dipeptidase derived from an environmental DNA sequence originally isolated from the Sargasso Sea (PDB code 2QS8) [31]. Additional homologues are the putative amidohydrolases Eaj56179 (3MKV, Z = 17.3 and RMSD 1.8 Å/362 Cα [30]) and Eah89906 (3FEQ and 3N2C, Z = 17.2 and RMSD = 1.8 Å/361 Cα; [30]), and the arginine carboxypeptidases Sgx9359b (3DUG, Z = 16.1 and RMSD = 1.8 Å/356 Cα; [29]) and Cc2672 (3MTW and 3BE7, Z = 14.9 and RMSD = 2.1 Å/352 Cα; [30]).

Superimposition of these homologues with OTapo-h, OTapo-l1 and OTholo-h (Figure 3) reveals highly similar core structures. Residues 466–480 of OTase have no equivalents because the sequences of the aligned amidohydrolases are shorter or their C-termini not resolved in the electron density map. Larger structural deviations are observed at the outmost periphery of the sandwich domain that face the bulk solvent or connect both domains. However, the most significant differences are seen between polypeptide stretches located at the top of the barrel, shaping the active site and the entrance to it (residues 118–129, 196–221, 251–259, 333–361 and 378–384). This includes ASS1 (residues 251–261) and ASS2 (residues 329–355), which adopt open and closed conformations or are partly disordered in the OTase structures (see below). Open ASS conformations are thus far unique to OTase as they have not been described for any of the homologous proteins [29–31].

The active site

The active site is formed by residues from the C-terminal ends of the barrel strands and the loops and helices directly downstream. In OTapo-h, OTapo-l1 and OTapo-l2, the active site constitutes a large and wide-open cavity that is easily accessible from the bulk solvent (Supplementary Figure S3A at http://www.biochemj.org/bj/462/bj4620441add.htm). The entrance to this cavity lies in the cleft between neighbouring dimeric units within the homo-octamer, placing those of diagonally adjacent protomers spatially close to one another. The active site of OTapo-h contains a number of water molecules, but no residual electron density indicative of covalent modification, metal ions or other ligands were observed. Nevertheless, the structural similarity and sequence conservation pattern to other members of the amidohydrolase family (Supplementary Figure S4 at http://www.biochemj.org/bj/462/bj4620441add.htm) indicated that OTase might require the presence of a binuclear metal centre and a carboxylated lysine residue for catalytic activity. Since the OTase batches used for crystallization showed catalytic activity that did not increase upon further addition of Zn^{2+} (results not shown), we assume that the metal ions dissociated during crystallization, possibly due to the presence of the mildly chelating citrate in the crystallization solution. Prominent bean-shaped positive electron density peaks were observed near histidines 287, 289 and 307 in the active sites of all eight subunits of OTapo-l1 and OTapo-l2, but the shape and dimensions do not correspond to a binuclear metal centre or any components of the utilized crystallization or purification solutions. The density is close to enzyme amine or amide nitrogen atoms, suggesting that the bound molecule contains carbonyl, carboxy and/or hydroxy groups. A citrate molecule from the crystallization solution would thus be the most likely candidate as a ligand, but it is too large to fit well into the density.

Although the OTapo-l2 crystal (space group *I*2) was grown in the presence of zinc ions and 4MF, neither metal centre binding nor Lys^{246} carboxylation were observed. This may be due to the relatively low pH of the crystallization solution rather than

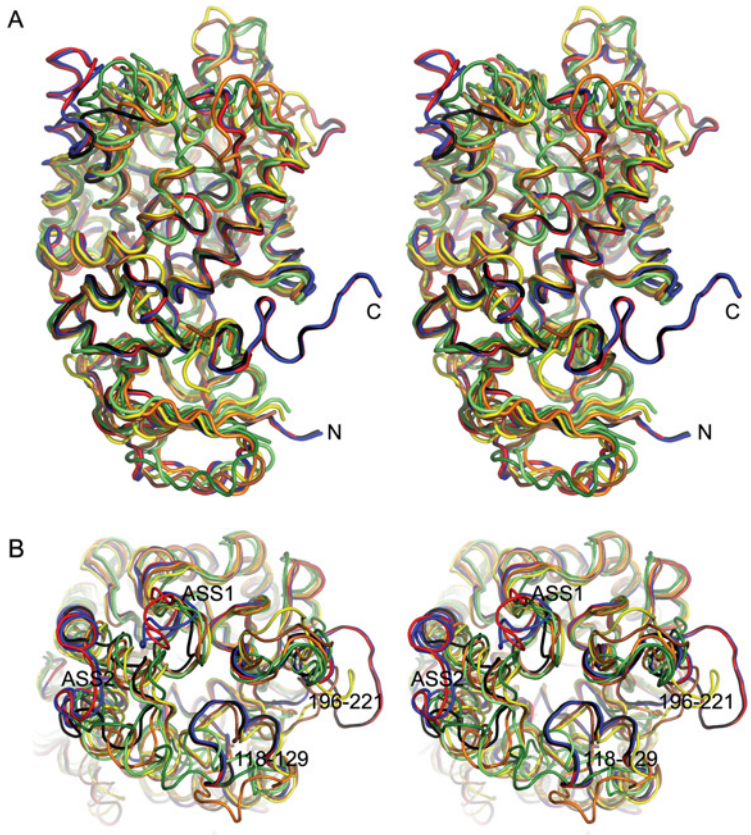

Figure 3 Superimposition of OTase with homologous enzymes

Black, OTholo-h; red, OTapo-h; blue, OTapo-l1; dark green, PDB-ID 2QS8; brown, 3N2C; orange, 3DUG; yellow, 3MKV; bright green, 3MTW. The structures of OTapo-l2 and PDB codes 3BE7 and 3FEQ are not depicted as they are highly similar to OTapo-l1 and PDB codes 3DUG and 3N2C respectively. (**A**) Stereo view showing the catalytic domain on top and the sandwich domain below. The OTase termini are labelled. (**B**) Top stereo view of the barrel domain, with amino acid stretches forming the entrance to the active site indicated.

the presence of the unknown ligand since the latter does not block the metal-binding site.

In contrast, soaking of a crystal of space group $P42_12$ grown at higher pH with Zn^{2+} ions and 4MF resulted in positive difference electron density peaks in the active site of OTholo-h at positions expected to be occupied by metal ions of a dinuclear centre. The relative weakness of these peaks and appearance of negative density after modelling of Zn^{2+} ions indicate that the metal sites are not fully occupied. Co-crystallization with $ZnCl_2$ as well as longer soaking times were therefore tested before subsequent diffraction tests, but whereas the former gave large, single and similarly well diffracting crystals only under the low-pH condition (e.g. OTapo-l2), the latter resulted in crystal cracking and/or poor diffraction properties. The (arbitrary) setting of the Zn^{2+} occupancies to 0.5 resulted in disappearance of the negative density peaks in subsequent refinements. The difference density map also revealed that Lys^{246} is carboxylated in OTholo-h, although no bicarbonate was added to the soaking solution. The covalent modification, modelled at full occupancy, promotes binding of Lys^{246} to both metal ions. In addition, the zinc ion at the site traditionally referred to as the α site is bound by His^{111} and His^{113}, whereas His^{287} and His^{307} co-ordinate Zn–β (Figures 4A and 4B). These residues are strictly conserved in homologous amidohydrolases (Supplementary Figure S4). There are no indications for the presence of a bridging hydroxy ion, probably due to the partial occupancy of the metal sites (Figure 4A).

Similar to OTapo-l1 and OTapo-l2, the active sites of OTholo-h harbour an unknown ligand (Figure 4A), but location and especially shape and size of the connected density do not exactly correspond to each other. For OTholo-h, it was tentatively modelled as phenylalanine, the hydrolysis product of the 4MF soaked into the crystals. However, whereas the main chain atoms fit well and make favourable hydrogen-bonding contacts with the surrounding enzyme residues the density observed for the phenyl side chain remains weak after refinement, indicating presence of a smaller amino acid, e.g. alanine or serine, or another ligand instead.

Conformational changes of ASS

Compared with the apoenzyme structures, OTholo-h shows altered conformations of ASS1 and ASS2 (Figure 4C and Supplementary Figure S3), with the former being folded down over the metal site to bind the unknown ligand. The open conformations observed for the apoenzyme in the two crystal forms are not fully equivalent: in OTapo-l1 and OTapo-l2 the first half of ASS1 is more open than in OTapo-h and the rest almost as closed as in OTholo-h. This may be caused by either the different pH of the crystallization solution or the presence of the unknown ligand in OTapo-l1 and OTapo-l2, but not OTapo-h. The diverse ASS1 conformations are primarily stabilized by interactions of Gly^{252}, Val^{253} and Asp^{258}. In the open state, the carboxy group

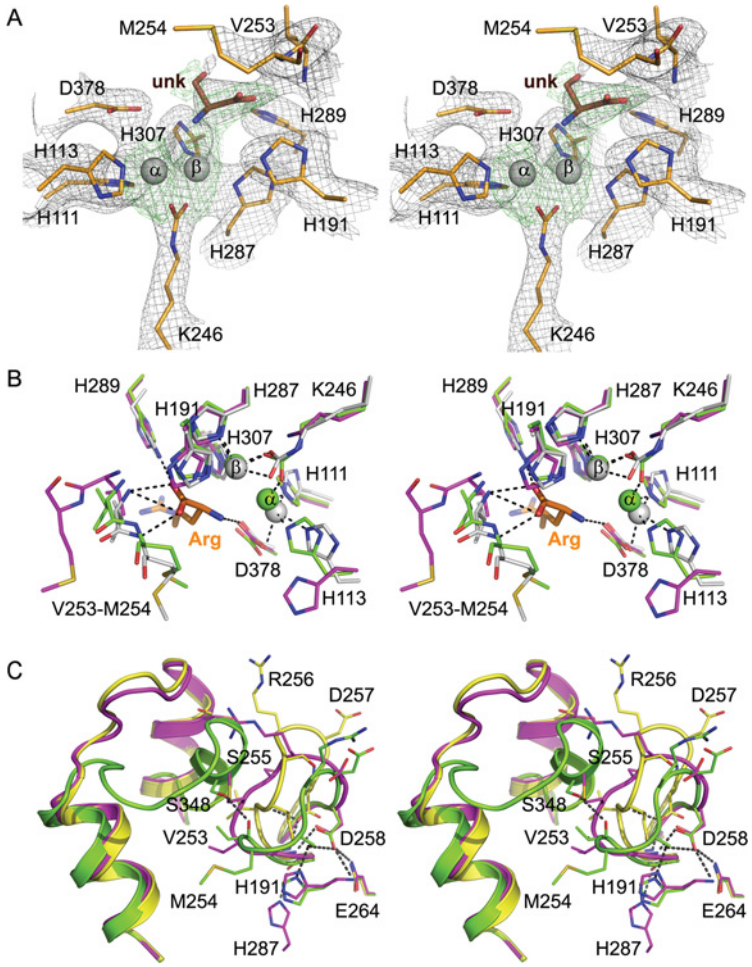

Figure 4 Active site and ASS conformational changes in apo- and holo-OTase

(**A**) Stereo view of the active site and observed electron density for OT-hZn. A $2F_o - F_c$ map (grey) is contoured at 1 σ in a 3 Å radius around the zinc ions, and a 2 Å radius around depicted residues. The $F_o - F_c$ map (green) obtained after refinement of a model from which both zinc ions and the covalent modification at Lys[264] were omitted is contoured at 3 σ. A serine was modelled into it the electron density for the unknown ligand (unk) to facilitate its identification in this Figure. (**B**) Stereo view of superimposed active site residues of OTapo-I1 (magenta), OTholo-h (green) and a product complex of arginine carboxypeptidase Sgx9359b (PDB code 3DUG; grey). Only OTase residues are labelled. The zinc ions of the di-metal centre are represented as green (OTholo-h) or grey spheres (Sgx9359b). The arginine molecule bound to Sgx9359b is shown with orange carbon atoms. Broken lines indicate metal co-ordination or hydrogen bonds to the ligand. (**C**) Stereo view of the superimposed ASSs of OTapo-h (yellow), OTholo-h (green) and OTapo-I1 (magenta). The loop conformations observed in OTapo-I2 correspond to those of OTapo-I1. Residue side chains are shown for all ASS1 residues and Ser[348] from ASS2. Hydrogen bonds are visualized as broken lines. To enhance clarity, side chains are labelled only once (for any one of the structures), and Gly[251] and Gly[252] of ASS1 are not labelled.

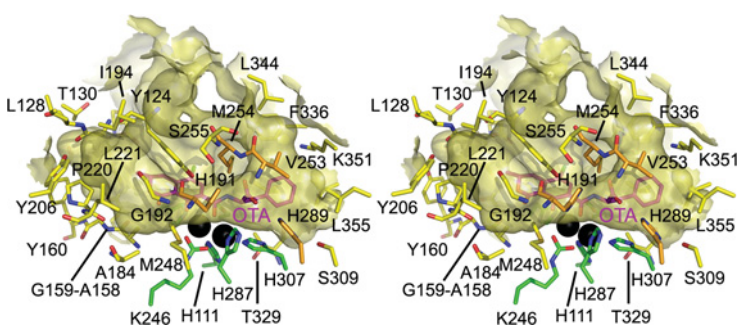

Figure 5 The substrate-binding cavity of OT-hZn

In the stereo figure, the cavity is outlined by the yellow-grey semi-transparent surface. The zinc ions are shown as black spheres. OTA was manually docked in the cavity and is depicted with purple carbon atoms. Zinc-binding, substrate–carboxylate/carbonyl group-binding and other residues lining the walls of the cavity are shown as sticks with green, orange and yellow carbon atoms respectively. Nitrogen, oxygen and sulfur atoms are depicted blue, red and bright orange respectively. For clarity, only residues in the foreground and at the sides of the cavity are labelled.

of Asp[258] is hydrogen bonded to Gly[252] and either Val[253] and Met[254] (OTapo-h) or Gln[264] and His[191] (OTapo-l1). In the closed state, the Asp[258] carboxy group interacts with the side chain of Ser[255] instead. At the other end of ASS1, Gly[252] and Val[253] are similarly positioned in all structures, but the hydrogen bond of Val[253] to the side chain of Ser[348] from ASS2 (and another likely one to the unknown ligand) is only observed in the holoenzyme. Here, the flip of residues 254–257 towards the metal centre moves the amide of Met[254] to a position close enough for interaction with the substrate/product carboxy group, whereas Ser[255] is moved by ~8 Å to form hydrogen bonds with Asp[258] and His[191].

The conformational change of ASS2 consisting of residues 329–355, i.e. α11, half of α12 and the loop connecting both helices, follows the movement of ASS1. In the apoenzyme structures, both helices are extending above the surface of the protein and the connecting loop is only six residues long (Figures 4C and Supplementary Figure S3). The absent or weak electron density for this loop indicates high intrinsic mobility. Formation of the holoenzyme–ligand complex causes a modest movement of α11 and a partial unwinding of the N-terminus of α12 (residues 345–353), which together with the connecting loop is folded downwards to form a roof over the active site.

We hypothesize that the presence of the metal centre is required, but not sufficient for closure of ASS1, based on that none of the residues interacts directly with a zinc ion or zinc-binding residue and that only the closed ASS1 conformation is observed for OTholo-h despite partial occupancy of the metal site. The closed state may instead be induced by substrate binding and stabilized by direct interactions of the backbone amides of Val[253] and Met[254] with the substrate. In contrast with ASS1, the conformational change of ASS2 does not occur in all molecules present in the OTholo-h crystal, as evident from the residual positive difference density fitting either one state after modelling and refinement of the other. Possibly the soaking time was insufficient to promote complete transformation. Open ASS conformations have not been reported for homologous enzymes (even if crystallized as apoenzymes) and are thus far a feature unique to *A. niger* OTase. The observation of the open state in two different crystal forms as well as of the open and closed state for the same crystal form does, however, indicate that it is not a crystallization artefact.

Substrate specificity and catalytic mechanism

In the closed state the substrate-binding pocket of OTase has a distinctly bi-lobar shape (Figure 5). The two lobes are connected by a tunnel large enough for placement of a scissile amide bond near the di-zinc centre. To date the natural substrate of OTase, if other than OTA, is unknown. The enzyme was selected for functional and structural studies based on its reactivity towards OTA. Reactivity and specificity for this major mycotoxin, 4MF, L-phenylalanyl-L-tyrosine, L-arginyl-L-phenylalanine and hippuryl-L-phenylalanine infers that the enzyme has a preference for phenylalanine residues or at least for a larger hydrophobic or aromatic moiety at the C-terminus, whereas the N-terminal moiety of the natural substrate(s) may be bulkier and partially polar. Accordingly, the cavity for the C-terminal half of the substrate is predominantly lined with hydrophobic residues, and that harbouring the N-terminal moiety is larger and of significantly more polar character (Figure 5). Tyr[124] would be suitably placed for π-stacking interactions with aromatic rings, whereas the side chains of Asp[117], Tyr[160], Ser[135], Tyr[124] and Tyr[206], and backbones of several other residues, may be hydrogen-bonding partners of the natural substrate(s) of OTase.

The presence of a dinuclear metal centre and the conservation of catalytic residues suggest that substrate hydrolysis follows a mechanism identical to that proposed for OTase homologues and other dinuclear amidohydrolases [43,44]. Cleavage is achieved by activation of a zinc-co-ordinated water molecule, which attacks the carbonyl carbon atom of the amide bond. This may be facilitated by the polarization of the carbonyl bond by co-ordination to a zinc ion and His[191], which will also stabilize the developing oxyanion. Protonation of the nascent amino group by Asp[378] leads to cleavage of the carbon–nitrogen bond.

A structure-based sequence alignment with homologous enzymes (Supplementary Figure S4) reveals that only the core catalytic machinery, i.e. His[191], Asp[378] and the zinc-binding residues, are strictly conserved. All aligned enzymes also show similar features for binding of a substrate carboxy group via the backbones of two active site residues (Val[253] and Met[254] in OTase), with one of them (Val[253]) being strictly conserved. As reported by Xiang et al. [30], the only side chain involved in binding of the substrate carboxylate is usually conserved as a histidine or a tyrosine (His[289] in OTase). The majority of the residues surrounding the cavities for the substrate moieties on the N- or C-terminal side of the scissile bond are not conserved between OTase and its homologues, indicating distinctly deviating substrate specificities.

In conclusion, we recombinantly produced both the putative amidase of *A. niger* UVK143, which is identical with the An14g02080 gene product of *A. niger* CBS 513.88, and the *A. nidulans* formamidase as active enzymes and revealed that they show no substrate specificity overlap. The putative amidase was identified as the OTA-hydrolysing component of the "Amano™ lipase" product and subsequently annotated as the first microbial ochratoxinase. The enzyme degrades OTA approximately 600-times more efficiently than bovine pancreatic CPA. Elucidation of its crystal structure identified it as a member of the amidohydrolase superfamily, thus extending the spectrum of enzymes of distinct folds and reaction mechanisms capable of hydrolysing the relatively bulky ochratoxins; whereas OTase employs a dimetal centre in catalysis, CPA uses a single zinc ion and carboxypeptidase Y uses a serine nucleophile. Its high efficacy and thermostability makes *A. niger* OTase a promising new agent for enzymatic detoxification of OTA-contaminated agricultural products.

AUTHOR CONTRIBUTION

Doreen Dobritzsch performed the structural analysis, interpreted the results and participated in the writing of the paper. Huaming Wang carried out cloning and expression experiments. Gunter Schneider provided expertise in crystallography and enzymology, and edited the paper before submission. Shukun Yu designed the research, performed the biochemical experiments, interpreted the results and participated in the writing of the paper.

ACKNOWLEDGEMENTS

We thank the European Synchrotron Radiation Facility (Grenoble, France), the EMBL Outstation at DESY (Hamburg, Germany) and MAX-lab (Lund, Sweden) for access to synchrotron radiation facilities and data collection support. This work was facilitated by access to the Protein Science Facility at Karolinska Institutet/Science for Life Laboratory Stockholm (http://psf.ki.se).

FUNDING

This work was supported by Danisco A/S. The Protein Science Facility is supported through funds from Karolinska Institutet, Science for Life Laboratory and the Swedish Research Council.

REFERENCES

1 Jelinek, C. F., Pohland, A. E. and Wood, G. E. (1989) Worldwide occurrence of mycotoxins in foods and feeds: an update. J. Assoc. Off. Anal. Chem. **72**, 223–230 PubMed

2 Duarte, S. C., Pena, A. and Lino, C. M. (2010) A review on ochratoxin A occurrence and effects of processing of cereal and cereal derived food products. Food Microbiol. **27**, 187–198 CrossRef PubMed

3 Abrunhosa, L., Paterson, R. R. M. and Venâncio, A. (2010) Biodegradation of ochratoxin A for food and feed decontamination. Toxins **2**, 1078–1099 CrossRef PubMed

4 EFSA (2004) Opinion of the Scientific Panel on Contaminants in Food Chain on a request from the Commission related to ochratoxin A (OTA) as undesirable substance in animal feed. EFSA J. **101**, 1–36

5 Lin, L., Chen, P., Fu, Y. and Shih, D. Y. (2005) Ochratoxin A contamination in coffees, cereals, red wines and beers in Taiwan. J. Food Drug. Anal. **13**, 84–92

6 Karlovsky, P. (1999) Biological detoxification of fungal toxins and its use in plant breeding, feed and food production. Nat. Toxins **7**, 1–23 CrossRef PubMed

7 Fuchs, S., Sontag, G., Stidl, R., Ehrlich, V., Kundi, M. and Knasmüller, S. (2008) Detoxification of patulin and ochratoxin A, two abundant mycotoxins, by lactic acid bacteria. Food Chem. Toxicol. **46**, 1398–1407 CrossRef PubMed

8 Péteri, Z., Téren, J., Vágvölgyi, C. and Varga, J. (2007) Ochratoxin degradation and adsorption caused by astaxanthin-producing yeasts. Food Microbiol. **24**, 205–210 CrossRef PubMed

9 Wu, Q., Dohnal, V., Huang, L., Kuča, K., Wang, X., Chen, G. and Yuan, Z. (2011) Metabolic pathways of ochratoxin A. Curr. Drug Metab. **12**, 1–10 CrossRef PubMed

10 Hwang, C. and Draughon, F. A. (1994) Degradation of ochratoxin A by *Acinetobacter calcoaceticus*. J. Food Protect. **57**, 410–414

11 Politis, I., Fegeros, K., Nitsch, S., Schatzmayr, G. and Kantas, D. (2005) Use of *Trichosporon mycotoxinivorans* to suppress the effects of ochratoxicosis on the immune system of broiler chicks. Brit. Poultry Sci. **46**, 58–65 CrossRef

12 Pitout, M. J. (1969) The hydrolysis of ochratoxin A by some proteolytic enzymes. Biochem. Pharmacol. **18**, 485–491 CrossRef PubMed

13 Stander, M. A., Steyn, P. S., van der Westhuizen, F. H. and Payne, B. E. (2001) A kinetic study into the hydrolysis of the ochratoxins and analogues by carboxypeptidase A. Chem. Res. Toxicol. **14**, 302–304 CrossRef PubMed

14 Doster, R. C. and Sinnhuber, R. O. (1972) Comparative rates of hydrolysis of ochratoxins A and B *in vitro*. Food Cosmet. Toxicol. **10**, 389–394 CrossRef PubMed

14a Pfohl-Leszkowicz, A. and Manderville, R. A. (2007) Ochratoxin A: an overview on toxocity and carcinogenicity in animals and humans. Mol. Nutr. Food Res. **51**, 61–99 CrossRef PubMed

15 Stander, M. A., Bornscheuer, U. T., Henke, E. and Steyn, P. S. (2000) Screening of commercial hydrolases for the degradation of ochratoxin A. J. Agric. Food Chem. **48**, 5736–5739 CrossRef PubMed

16 Abrunhosa, L., Santos, L. and Venâncio, A. (2006) Degradation of ochratoxin A by proteases and by a crude enzyme of *Aspergillus niger*. Food Biotechnol. **20**, 231–242 CrossRef

17 Abrunhosa, L. and Venâncio, A. (2007) Isolation and purification of an enzyme hydrolyzing ochratoxin A from *Aspergillus niger*. Biotechnol. Lett. **29**, 1909–1914 CrossRef PubMed

18 Ward, M., Wilson, L. J. and Kodama, K. H. (1993) Use of *Aspergillus* overproducing mutants, cured for integrated plasmid, to overproduce heterologous proteins. Appl. Microbiol. Biotechnol. **39**, 738–743 CrossRef PubMed

19 Pel, H. J., de Winde, J. H., Archer, D. B., Dyer, P. S., Hofmann, G., Schaap, P. J., Turner, G., de Vries, R. P., Albang, R., Albermann, K. et al. (2007) Genome sequencing and analysis of the versatile cell factory *Aspergillus niger* CBS 513.88. Nat. Biotechnol. **25**, 221–231 CrossRef PubMed

20 Wang, H. (2002) Phenol oxidizing enzymes. U.S. Pat. 6426410 (B1)

21 Berka, R. M., Ward, M., Wilson, L. J., Hayenga, K. J., Kodama, K. H., Carlomagno, L. P. and Thompson, S. A. (1990) Molecular cloning and deletion of the gene encoding aspergillopepsin A from *Aspergillus awamori*. Gene **86**, 153–162 CrossRef PubMed

22 Campbell, E. I., Unkles, S. E., Macro, J. A., van den Hondel, C., Contreras, R. and Kinghorn, J. R. (1989) Improved transformation efficiency of *Aspergillus niger* using the homologous *niaD* gene for nitrate reductase. Curr. Genet. **16**, 53–56 CrossRef PubMed

23 Fraser, J. A., Davis, M. A. and Hynes, M. J. (2001) The formamidase gene of *Aspergillus nidulans*: Regulation by nitrogen metabolite repression and transcriptional interference by an overlapping upstream gene. Genetics **157**, 119–31 PubMed

24 Abrunhosa, L., Serra, R. and Venâncio, A. (2002) Biodegradation of ochratoxin A by fungi isolated from grapes. J. Agric. Food Chem. **50**, 7493–7496 CrossRef PubMed

25 Leslie, A. G. W. and Powell, H. R. (2007) Processing diffraction data with MOSFLM. In Evolving Methods for Macromolecular Crystallography (Read, R. J. and Sussman, J. L., eds), pp. 40–52, Springer, Dordrecht

26 Evans, P. R. (2011) An introduction to data reduction: space-group determination, scaling and intensity statistics. Acta Crystallogr. D Biol. Crystallogr. **67**, 282–292 CrossRef PubMed

27 Winn, M. D., Ballard, C. C., Cowtan, K. D., Dodson, E. J., Emsley, P., Evans, P. R., Keegan, R. M., Krissinel, E. B., Leslie, A. G., McCoy, A. et al. (2011) Overview of the CCP4 suite and current developments. Acta Crystallogr. D Biol. Crystallogr. **67**, 235–242 CrossRef PubMed

28 McCoy, A. J., Grosse-Kunstleve, R. W., Adams, P. D., Winn, M. D., Storoni, L. C. and Read, R. J. (2007) Phaser crystallographic software. J. Appl. Crystallogr. **40**, 658–674 CrossRef PubMed

29 Xiang, D. F., Patskovsky, Y., Xu, C., Meyer, A. J., Sauder, J. M., Burley, S. K., Almo, S. C. and Raushel, F. M. (2009) Functional identification of incorrectly annotated prolidases from the amidohydrolase superfamily of enzymes. Biochemistry **48**, 3730–3742 CrossRef PubMed

30 Xiang, D. F., Patskovsky, Y., Xu, C., Fedorov, A. A., Fedorov, E. V., Sisco, A. A., Sauder, J. M., Burley, S. K., Almo, S. C. and Raushel, F. M. (2010) Functional identification and structure determination of two novel prolidases from cog1228 in the amidohydrolase superfamily. Biochemistry **49**, 6791–6803 CrossRef PubMed

31 Xiang, D. F., Xu, C., Kumaran, D., Brown, A. C., Sauder, J. M., Burley, S. K., Swaminathan, S. and Raushel, F. M. (2009b) Functional annotation of two new carboxypeptidases from the amidohydrolase superfamily of enzymes. Biochemistry **48**, 4567–4576 CrossRef

32 Emsley, P., Lohkamp, B., Scott, W. G. and Cowtan, K. (2010) Features and development of Coot. Acta Crystallogr. D Biol. Crystallogr. **66**, 486–501 CrossRef PubMed

33 Murshudov, G. N., Vagin, A. A. and Dodson, E. J. (1997) Refinement of macromolecular structures by the maximum-likelihood method. Acta Crystallogr. D Biol. Crystallogr. **53**, 240–255 CrossRef PubMed

34 Lovell, S. C., Davis, I. W., Arendall, W. B., de Bakker, P. I. W., Word, J. M., Prisant, M. G., Richardson, J. S. and Richardson, D. C. (2003) Structure validation by Calpha geometry: phi, psi and Cbeta deviation. Proteins **50**, 437–450 CrossRef PubMed

35 Chen, V. B., Arendall, W. B., Headd, J. J., Keedy, D. A., Immormino, R. M., Kapral, G. J., Murray, L. W., Richardson, J. S. and Richardson, D. C. (2010) MolProbity: all-atom structure validation for macromolecular crystallography. Acta Crystallogr. D Biol. Crystallogr. **66**, 12–21 CrossRef PubMed

36 Kabsch, W. (1976) A solution for the best rotation to relate two sets of vectors. Acta Crystallogr. A **32**, 922–923 CrossRef

37 Krissinel, E. and Henrick, K. (2004) Secondary-structure matching (SSM), a new tool for fast protein structure alignment in three dimensions. Acta Crystallogr. D Biol. Crystallogr. **60**, 2256–2268 CrossRef PubMed

38 Krissinel, E. and Henrick, K. (2007) Inference of macromolecular assemblies from crystalline state. J. Mol. Biol. **372**, 774–797 CrossRef PubMed

39 Dundas, J., Ouyang, Z., Tseng, J., Binkowski, A., Turpaz, Y. and Liang, J. (2006) CASTp: computed atlas of surface topography of proteins with structural and topographical mapping of functionally annotated residues. Nucleic Acids Res. **34**, W116–W118 CrossRef PubMed

40 Wang, H. (2010) Increased production of aspartic proteases in filamentous fungal cells. U.S. Pat. WO2010014574 (A3)

41 Streekstra, H. (2006) Amidases from *Aspergillus niger* and their use in a food production process. U.S. Pat. 11/664,419

42 Futagami, T., Mori, K., Yamashita, A., Wada, S., Kajiwara, Y., Takashita, H., Omori, T., Takegawa, K., Tashiro, K., Kuhara, S. and Goto, M. (2011) Genome sequence of the white koji mold *Aspergillus kawachii* IFO 4308, used for brewing the Japanese distilled spirit shochu. Eukaryot. Cell **10**, 1586–1587 CrossRef PubMed

43 Seibert, C. M. and Raushel, F. M. (2005) Structural and catalytic diversity within the amidohydrolase superfamily. Biochemistry **44**, 6383–6391 CrossRef PubMed

44 Thoden, J. B., Phillips, Jr, G. N., Neal, T. M., Raushel, F. M. and Holden, H. M. (2001) Molecular structure of dihydroorotase: a paradigm for catalysis through the use of a binuclear metal center. Biochemistry **40**, 6989–6997 CrossRef PubMed

Received 23 March 2014/10 June 2014; accepted 20 June 2014
Published as BJ Immediate Publication 20 June 2014, doi:10.1042/BJ20140382

Biochem. J. (2014) **462**, 441–452 (Printed in Great Britain) doi:10.1042/BJ20140382

SUPPLEMENTARY ONLINE DATA

Structural and functional characterization of ochratoxinase, a novel mycotoxin-degrading enzyme

Doreen DOBRITZSCH*†[1], Huaming WANG‡§, Gunter SCHNEIDER* and Shukun YU¶‖[1]

*Department of Medical Biochemistry and Biophysics, Karolinska Institutet, SE-17177 Stockholm, Sweden
†Department of Chemistry, BMC, Uppsala University, SE-75123 Uppsala, Sweden
‡Genencor, Danisco A/S (DuPont), Palo Alto, CA 94304, U.S.A.
§Tianjin Institute of Industrial Biotechnology, Chinese Academy of Science, 300308 Tianjin, China
¶Genencor, Danisco A/S (DuPont), DK-8220 Brabrand, Denmark
‖Department of Biotechnology, Lund University, SE-22100 Lund, Sweden

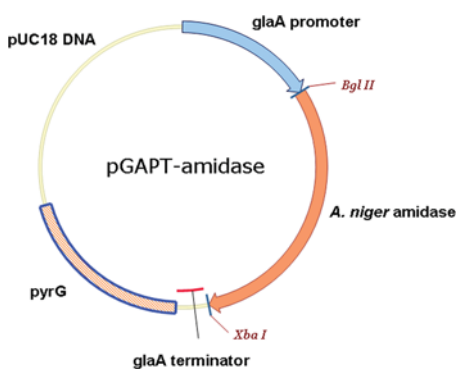

Figure S1 Plasmid map for the *A. niger* amidase (OTase) expression vector pGAPT-amidase

[1] Correspondence may be addressed to either of these authors (email Doreen.Dobritzsch@kemi.uu.se or Shukun.Yu@biotek.lu.se).

The crystallographic data and structures described in the present paper have been deposited in the PDB under codes 4C5Z (OTapo-h), 4C5Y (OTholo-h), 4C60 (OTapo-l1) and 4C65 (OTapo-l2).

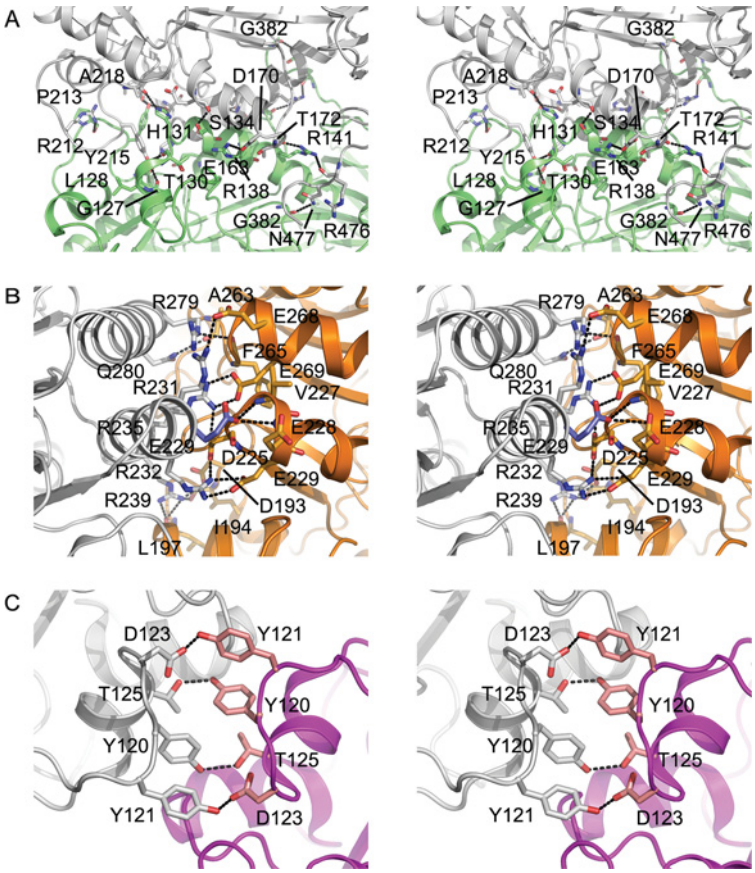

Figure S2 Inter-subunit interfaces in the *A. niger* OTase homo-octamer

The polypeptide chains of the interacting subunits are shown in cartoon representation and coloured as in Figure 2(B) of the main text. The grey subunit is in contact with its dimer mate (bright green), its neighbours in the half-tetramer formed by four-fold symmetry (blue and orange), and the dimer mate of the blue subunit (magenta). Hydrogen bonds and salt bridges are visualized by broken lines; the involved residues are shown with carbon atoms in a colour similar to that of the respective subunit. (**A**) Stereo view of the interface between dimer mates. The two-fold axis relating both subunits lies approximately in the paper plane, running diagonally from the top left to the bottom right corner. Accordingly, the same residues from both subunits are involved in formation of this interface, but for clarity only one set is labelled. (**B**) Stereo view of the subunit interface in a half-tetramer assembled by four-fold symmetry. The Figure depicts the interaction between the subunits shown as grey and orange in Figure 2(B) of the main text, but is also representative for the interface between the grey and blue subunits. The buried surface patch of one subunit is dominated by positively charged amino acids, in particular arginine residues, which is complemented by a number of negatively charged residues (aspartate and glutamate) on the surface of the interacting subunit. (**C**) Stereo view of the interface between diagonally opposite subunits of two neighbouring dimers, which are related by two-fold symmetry. Here, all hydrogen bonds involve tyrosine residues.

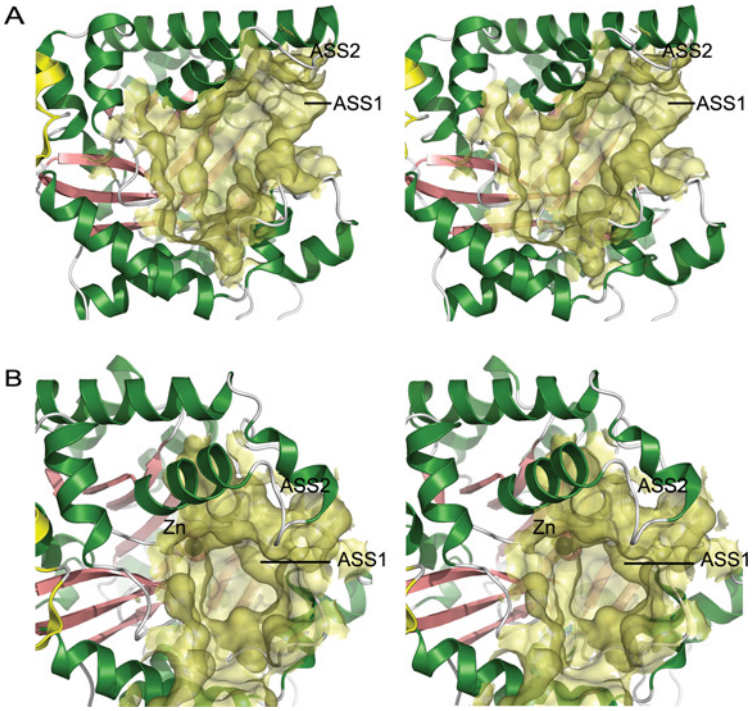

Figure S3 Active site cavities

Stereo views of the active site cavities of OTapo-I1 (**A**) and OTholo-h (**B**), with their dimensions outlined by a partial molecular envelop in yellow-grey. ASSs are labelled. The zinc ions bound to the holoenzyme are shown as black spheres (in the chosen orientation one of them is concealed by the other).

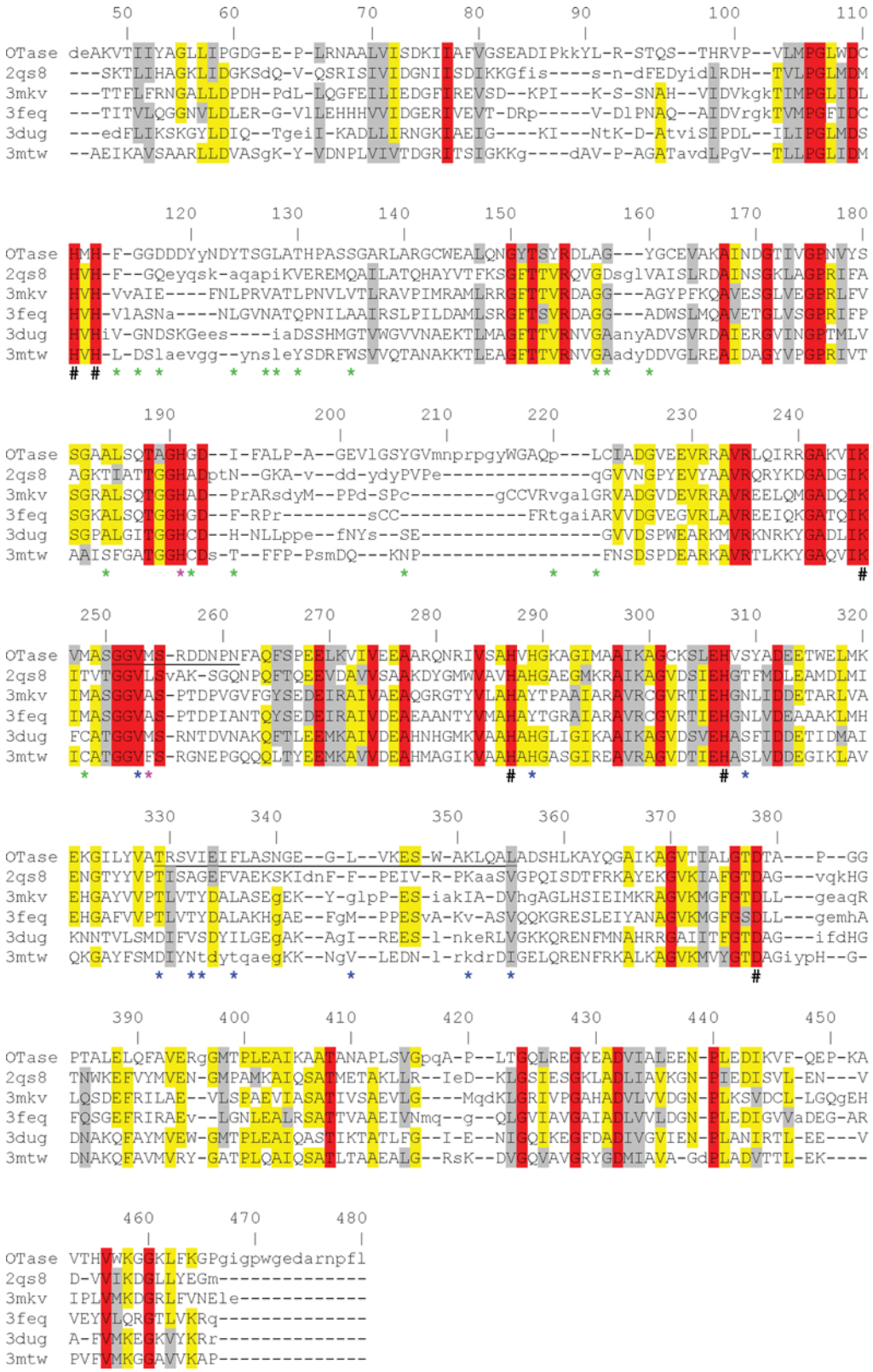

Figure S4 Structure-based sequence alignment of *A. niger* OTase and homologous peptidases and amidohydrolases

The sequences of the OTase homologues are listed with their respective PDB codes. Capital letters indicate regions that can be structurally aligned to OTase (OT-hZn). Strictly conserved amino acid residues are highlighted by a red background, residues that are conserved in the majority of the sequences are shown with a yellow background. Grey background indicates conservation of the side chain properties in at least five of the six sequences. OTase regions corresponding to ASS1 and ASS2 are underlined. Zinc-ligating residues are marked by #, amino acids lining the cavities for the N- and C-terminal halves of the substrate, or both, are marked by asterisks in green, blue and magenta respectively.

Table S1 Subunit interactions in *A. niger* OTase (OTapo-I1)

In Figure 2(B) of the main text and Figure S2, subunits 1–5 are shown in grey, bright green, blue, orange and magenta respectively.

Interface I					
Buried solvent-accessible surface area					
Subunit 1: ~1910 Å^2 (10.2%)			Subunit 2: ~1910 Å^2 (10.2%)		
Interface residues					
Subunit 1: 116, 118, 119, 127-142, 144, 145, 149, 160, 163, 164, 166, 167, 170-174, 200, 201, 204-206, 212-215, 218, 220, 379-384, 450, 470, 471, 475-480			Subunit 2: 116, 118, 119, 127-134, 136-142, 144, 145, 149, 160, 163, 164, 166, 167, 170-174, 200, 201, 204-206, 212-215, 218, 220, 379-384, 450, 470, 471, 475-480		
Hydrogen bonds			**Salt bridges**		
Atom (Subunit 1)	Atom (Subunit 2)	Distance [Å]	Atom (Subunit 1)	Atom (Subunit 2)	Distance [Å]
L128-O	Y215-OH	2.8	R138-Nε	D170-Oδ2	2.9
T130-O	Y215-OH	2.7	R138-Nη2	D170-Oδ2	2.9
H131-Nε2	A218-O	2.8	D170-Oδ2	R138-Nε	2.9
S134-Oγ	E163-O	2.6	D170-Oδ2	R138-Nη2	3.0
R138-Nε	D170-Oδ2	2.9			
R138-Nη2	D170-Oδ2	2.9			
R141-Nη2	T172-O	2.8			
R141-Nη1	R476-O	3.0			
E163-O	S134-Oγ	2.6			
D170-Oδ2	R138-Nε	2.9			
D170-Oδ2	R138-Nη2	3.0			
T172-O	R141-Nη2	2.8			
R212-Nη2	P213-O	3.4			
Y215-OH	L128-O	2.8			
Y215-OH	T130-O	3.0			
A218-O	H131-Nε2	3.0			
G382-O	N477-Nδ2	2.9			
R476-O	R141-Nη1	3.0			
N477-Nδ2	G382-O	2.7			
Interface II/III					
Buried solvent-accessible surface area					
Subunit 1/4: ~940 Å^2 (5.0%)			Subunit 3/1: ~1070 Å^2 (5.7%)		
Interface residues					
Subunit 1/4: 187-189,193-195, 197-204, 209, 210, 223, 225-229, 258-259, 262-269, 347			Subunit 3/1: 208-217, 228, 231, 232, 235, 236, 238, 239, 275, 276, 279-282, 418		
Hydrogen bonds			**Salt bridges**		
Atom (Subunit 1/4)	Atom (Subunit 3/1)	Distance [Å]	Atom (Subunit 1/4)	Atom (Subunit 3/1)	Distance [Å]
D193-Oδ2	R239-Nε	2.6	D193-Oδ1	R239-Nε	3.6
D193-Oδ1	R239-Nη1	2.7	D193-Oδ1	R239-Nη1	2.7
I194-O	R239-Nη1	2.8	D193-Oδ2	R239-Nε	2.6
L197-O	R239-Nη1	3.1	D193-Oδ2	R239-Nη1	3.4
L197-O	R239-Nη2	2.8	D225-Oδ1	R235-Nη1	2.9
D225-Oδ2	R232-Nη1	2.8	D225-Oδ1	R235-Nε	4.0
D225-Oδ1	R235-Nη1	2.9	D225-Oδ2	R232-Nη1	2.8
V227-N	E228-Oε1	2.9	D225-Oδ2	R232-Nε	4.0
E228-N	E228-Oε1	3.2	E229-Oε1	R232-Nη1	3.2
E229-Oε2	R232-Nη1	3.0	E229-Oε1	R232-Nη2	2.7
E229-Oε1	R232-Nη2	2.7	E229-Oε2	R232-Nη1	3.0
A263-O	Q280-Nε2	3.3	E229-Oε2	R232-Nη2	3.9
E269-Oε1	R235-Nη1	3.0	E269-Oε1	R235-Nη1	3.0
E269-Oε2	R235-Nη2	2.7	E269-Oε1	R235-Nη2	3.5
			E269-Oε2	R235-Nη1	3.7
			E269-Oε2	R235-Nη2	2.7
Interface IV					
Buried solvent-accessible surface area					
Subunit 1: ~480 Å^2 (2.6%)			Subunit 5: ~470 Å^2 (2.6%)		
Interface residues					
Subunit 1: 120, 121, 123, 125, 128, 129, 196-198, 201, 205, 256			Subunit 5: 120, 121, 123, 125, 128, 129, 196-198, 201, 205, 256		
Hydrogen bonds			**Salt bridges**		
Atom (Subunit 1)	Atom (Subunit 5)	Distance [Å]	Atom (Subunit 1)	Atom (Subunit 5)	Distance [Å]
Y120-OH	D123-Oδ2	2.5			
Y121-OH	T125-Oγ1	2.9			
D123-Oδ2	Y120-OH	2.6			
T125-Oγ1	Y121-OH	3.0			

Received 23 March 2014/10 June 2014; accepted 20 June 2014
Published as BJ Immediate Publication 20 June 2014, doi:10.1042/BJ20140382